Designs for a compact Ni-like-tungsten x-ray laser

Chris D. Decker and Richard A. London
Lawrence Livermore National Laboratory, Livermore, California 94550
(Received 19 February 1997; revised manuscript received 18 August 1997)

We propose a scheme for a compact nickel-like-tungsten soft-x-ray laser operating on the $4d$-$4p$, $J=0$-1 transition at 43.2 Å. High gains are achieved by operating at high electron densities ($n_e > 10^{22}$ cm^{-3}). In this regime, the gain during nonequilibrium ionization can greatly exceed that of the steady state. The duration of this transient gain is on the order of the ionization time, which makes picosecond-pulsed optical pumps ideal. Two target designs, solid tungsten slabs, and tungsten aerogels foams, are considered. We predict gains of 220 cm^{-1} for a 1-μm pump of intensity $I=2.5\times10^{16}$ W/cm^2.
[S1050-2947(98)06602-5]

PACS number(s): 42.55.Vc, 32.80.Rm, 52.75.Va

I. INTRODUCTION

Over the past decade significant progress has been made in the area of laser-driven collisionally excited soft-x-ray lasers [1,2]. In particular, Ni-like lasers have been proposed [3,4] and demonstrated [2,5] to operate in and near the ''water window.'' Wavelengths within the water window (23–44 Å) are of interest for microscopy of biological samples owing to the contrast between water and carbon containing substances (proteins, DNA, etc.). Wavelengths just longer than the carbon K edge are also of interest . For x-ray holography, the maximum scattering of carbon containing structures in water is expected to be just above 44 Å [6]. This is also a good wavelength for imaging gold-tagged biological specimens [7] and for the use of carbon containing multilayer mirrors for the optical elements of an imaging system. Although current Ni-like systems can access the water window, the required driver energy restricts these to a few large facilities. In order to have a practical x-ray laser for small laboratory operation, the size and cost of the driving laser must be reduced.

Recent advances in short-pulse high-intensity optical lasers have led to numerous table-top systems throughout the world. As a result, there have been efforts aimed at trying to use these compact optical lasers as drivers for x-ray lasers. The short-pulse lengths (subpicosecond) of these drivers make them inappropriate for the conventional exploding foil [8]-type designs, which require nanosecond pumps. Therefore, different schemes must be employed. Collisionally excited Ne-like [9] and recombination x-ray lasers [10] driven by short-pulse systems both have been demonstrated. However, the x-ray wavelengths for these schemes are well above the water window. Different schemes that operate below the water window such as inner-shell photoionization are needed and currently being investigated [11].

In order to utilize the short-pulse technology we must rely on an x-ray laser scheme that operates on picosecond time scales. High gains in Ne-like systems recently have been predicted to exist in a transient regime [12]. Such a regime has been proposed for collisionally excited Ni-like lasers at high electron density ($n_e > 10^{22}$ cm^{-3}) [13]. In this regime, the high electron density results in high excitation rates and leads to significant populations inversion. However, the high electron density also results in large ionization rates and the material becomes overionized (past Ni-like) on time scales of the order of 1 ps.

We propose to use the high gain of this transient regime for a compact Ni-like W x-ray laser using the $4d$-$4p$ (43.2 Å) $J=0$-1 transition. Details about the energy levels for Ni-like W can be found in Ref. [4]. In this paper we present results from fully integrated design calculations using sophisticated codes and atomic data bases established at the Lawrence Livermore National Laboratory. Designs are based on current and near term short-pulse high-intensity optical laser systems. Although the specific design calculations described in this paper are for W, they can be applied to Ta (44.8 Å) as well. In order to characterize this transient gain regime, we first focus on just the atomic kinetics. Next, we turn our attention to fully integrated target designs. From these target design studies we are able to estimate the gain length product as well as pump energy requirements. In addition, we examine the various experimental challenges anticipated with such a short-wavelength transient scheme.

II. LOCAL GAIN CALCULATIONS

Throughout this study, gain calculations were performed using the atomic kinetics code CRETIN [14]. The code solves for time-dependent level populations including such processes as electron collisional excitation and ionization, photoexcitation, and ionization, Auger excitation and ionization, and the inverses of these processes. The spectral widths are calculated from Doppler and lifetime broadening (including both radiative decay and inelastic collisions). For the conditions presented here we find a relative linewidth ratio ($\Delta\lambda/\lambda$) around 4×10^{-4}, dominated by lifetime broadening. We estimate the Stark width [15] to be about 1/4 of this width and therefore ignored the stark width in the gain. The atomic model includes 39 ionization stages from Nd-like to Ti-like. The Ni-like stage has 197 detailed levels and 30 Rydberg states (up to $n=10$).

In order to understand the time-dependent behavior associated with the atomic kinetics we first perform ''zero-dimensional'' (0D) calculations. In these 0D calculations the electron temperature T_e and ion (material) density ρ were specified and held constant over time. The atomic popula-

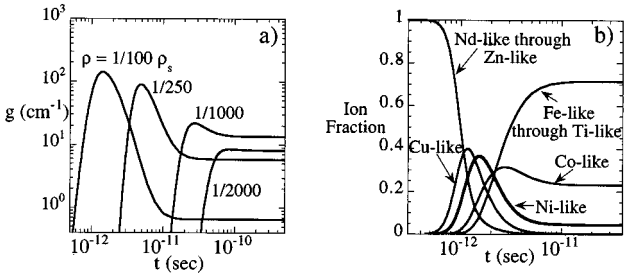

FIG. 1. (a) Gain coefficient vs time at several material densities for $T_e = 1.0$ keV and $T_i = 0.1$ keV. (b) Ion fractions versus time for the $\rho = 1/100\rho_s$ case.

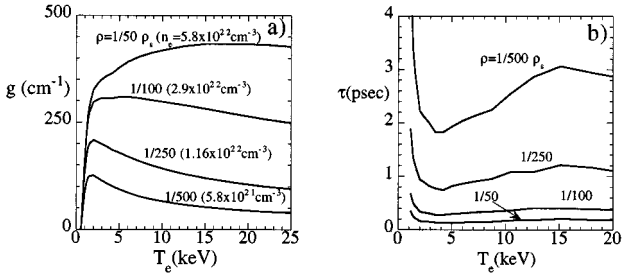

FIG. 2. (a) Peak gain coefficient vs T_e ($T_i = T_e/10$) at several material densities. (b) Gain duration versus electron temperature.

tions, however, evolve in time and result in time-dependent gains. The material is initialized in a very low ionization stage (Nd-like).

To illustrate this high-density regime and contrast it with the conventional low-density steady-state regime, we plot the gain versus time for several ion densities in Fig. 1(a) for $T_e = 1.0$ keV and $T_i = 0.1$ keV. The curves are labeled according to the density relative to solid density ρ_s. For tungsten $\rho_s = 19.35$ g/cm^3. First, we consider the lowest density case of $\rho = 1/2000\rho_s$. For this electron temperature, the steady-state electron density is $n_e = 1.25 \times 10^{21}$ cm^{-3}. These conditions are very similar to those in conventional long-pulse exploding foil Ni-like x-ray lasers [4]. For this case the gain turns on after about 40 ps and reaches its steady state value of 8.7 cm^{-1} in about 100 ps. For this reason, the low density exploding foil designs require long (100-ps) pump pulses. Next, we consider an intermediate density case of $\rho = 1/250\rho_s$. Here the gain rises rapidly to 91 cm^{-1} in several picoseconds. At about 5 ps the large ionization rate starts to reduce the Ni-like abundance and the gain drops until the steady state value of 6.3 cm^{-1} is reached in about 20 ps. Finally, we consider the high-density regime of $\rho = 1/100\rho_s$. For this case a peak gain of 152 cm^{-1} occurs at a time of approximately 1 ps. The electron density at peak gain is $n_e = 2.9 \times 10^{22}$ cm^{-3}. After 3 ps the material becomes overionized and the steady-state gain drops to 0.7 cm^{-1}, which is much smaller than the lower-density cases. The pulse length is determined from the ionization rates for the high density regime. To see this we plot the ionization fractions in Fig. 1(b). We show the Co-like, Ni-like, and Cu-like stages, the sum of all stages above the Co-like stage, and the sum of all stages below the Cu-like stage. The peak gain coincides with the peak Ni-like abundance of 37%.

It is evident from the gain curves shown in Fig. 1(a) for the high-density cases that we can define a peak gain g_p and a full width at half maximum of the gain duration τ. A series of calculations were performed varying the material density and electron temperature. The results are shown in Fig. 2, where we plot g_p and τ versus electron temperature for $\rho = 1/50$, $1/100$, $1/250$, and $1/500$ ρ_s. Hydrodynamical simulations including laser absorption show low ion temperatures. For this reason, we held $T_i = T_e/10$ while T_e was varied. Because of the time-dependent ionization, the electron density changes with time at constant mass density. Therefore, we give the electron densities at peak gain in parentheses. We note that for all densities there is a minimum electron temperature of about 1 keV required in order to have an appreciable monopole excitation rate that is the dominant process populating the upper lasing level. Although higher gain always occurs for higher electron density, the optimal electron density is limited by target coupling and x-ray propagation issues that will be discussed below. However, from Fig. 2(b) it is obvious that we need to operate at electron temperatures in excess of 1 keV. From Fig. 2(b) we see that the gain durations are in the picosecond regime and they decrease rapidly with density.

III. INTEGRATED DESIGNS

Having examined the atomic kinetics, we now turn our attention to fully integrated target designs. Design calculations including laser absorption, hydrodynamic expansion, and heat wave propagation were performed with the radiation hydrodynamic code LASNEX [16]. Although LASNEX can determine the laser absorption self-consistently via inverse bremsstrahlung, the calculated absorption fractions do not agree with experimental values at high intensities $I \geqslant 10^{16}$ W/cm^2 [17,18]. The discrepancy has been attributed to noncollisional effects [18]. Therefore, to obtain the highest level of confidence in our designs we use experimentally observed absorption fractions in the calculations.

We first consider solid tungsten slab targets. In order to relax density gradients that can severely limit the gain length by refracting x rays out of the gain region, the main driving pulse must be preceded by a low-intensity prepulse [19]. The prepulse allows for hydrodynamical expansion, which reduces the density gradient. However, there is a limit on how much expansion can be tolerated. Since we are interested in densities that are above the critical density, the energy must be deposited near critical density and transported to the higher-density gain region. In long-scale-length plasmas it is difficult to couple energy from the absorption region to the desired gain region. Therefore, the optimal prepulse conditions must be found.

Numerous 1D hydrodynamical simulations using LASNEX were performed. The resulting time-dependent density and temperature profiles were then fed into CRETIN and the gain coefficient as a function of space and time was obtained. Since radiation trapping may be important we included transfer of the lines with the strongest oscillator strengths. We found that a prepulse duration of 40–50 ps gave the highest gain values. Shown in Fig. 3 are the results from a simulation of a flat 40-ps prepulse of intensity 10^{14} W/cm^2 followed by a (2.5×10^{16})-W/cm^2, 1-ps Gaussian pulse. Since the coupling is best when the laser deposition region is closest to the

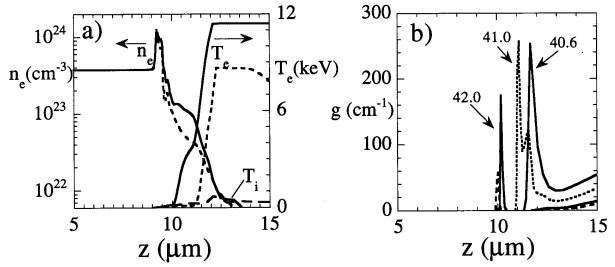

FIG. 3. Simulation results for a solid slab tungsten target. (a) Electron density and temperature at $t=40.5$ ps (dashed lines) and $t=41.5$ ps (solid lines). (b) Gain profiles at several times.

gain region the wavelength was chosen to be 0.25 μm. The assumed absorption fraction was 40%. We note that absorption fractions greater than 40% have been observed at this intensity and wavelength [18]. However, simulations [18] show that some of the absorbed energy, at these high intensities, goes into hot electrons, which may not couple into the gain region. The tungsten slab extends from 0 to 10 μm and the laser is incident from the right. In Fig. 3(a) we show the electron density and temperature at $t=40.5$ ps (dashed lines) and $t=41.5$ ps (solid lines). The resulting gain profiles are shown in Fig. 3(b). The peak gain occurs at $t=41$ ps around an electron density of 3×10^{22} cm^{-3} and an electron temperature of 4 keV. The ion density at this point corresponds to 1/100 solid and Fig. 2(a) shows that this temperature is near optimal for the 1/100 solid density case. However, the narrow spatial extent of the gain (0.4 μm) could be a limiting factor. We can estimate the distance as the photon travels before it refracts out of the gain region using geometrical optics. The angular deflection after traveling a distance L is given by

$$\delta\theta=\frac{1}{2}\int_0^L\nabla(n_e/n_c)\approx\frac{L}{2}\nabla(n_e/n_c), \tag{1}$$

where n_e is the electron density and n_c is the critical density for 43.2-Å radiation. A photon will refract out of a gain region of width δz when $\delta z=\delta\theta L$. Substituting this condition into Eq. (1), we find that the maximum length for gain before photons leave the gain region is given by

$$L=\sqrt{\frac{2\,\delta z}{\nabla(n_e/n_c)}}. \tag{2}$$

From the LASNEX simulations we find $\nabla(n_e/n_c)\sim4\times10^{-4}$ μm^{-1} over the gain region. Using this value for the density gradient along with $\delta z=0.4$ μm, we find $L=50$ μm, which gives a gain length product of about $GL=\leqslant1$. In order to obtain a measurable signal the refraction problem must be solved. One solution is to use a curved Lunney-type target [20]. In such a target, the surface is curved to follow the trajectory of the refracting x rays. Using the calculated density gradient, we estimate the radius of curvature needed to overcome refraction is approximately 2.5 mm.

Curved targets reduce refraction losses when density gradients occur. Obviously, a more direct solution is to reduce the density gradients. With solid targets large density gradients will always exist because the density of the gain region

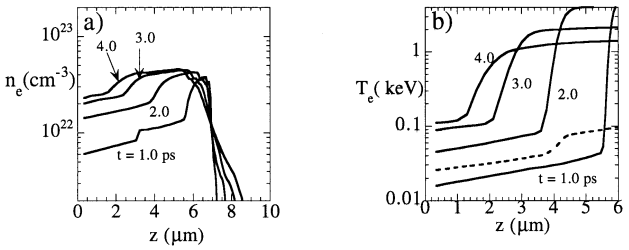

FIG. 4. Simulation results for a $\rho=0.23$ g/cm^3 tungsten aerogel. (a) Electron density at various times and (b) electron temperature at several times and the ion temperature (dashed line) at 2.0 ps.

is less than solid density and must be produced through hydrodynamical expansion. However, if the target could be prepared at the desired density, hydrodynamical expansion would not be necessary. Therefore, we propose the use of low-density targets. A promising target material is an aerogel foam. Aerogels are made by a solution-gel polymerization process. They can be fabricated of a variety of metal oxides, with densities in the range 0.03–0.6 g/cm^3 and pore sizes between 20 and 50 nm [22]. In particular, aerogels of Ta_2O_5 have already been made at the Lawrence Livermore National Laboratory and it should be possible to make W_2O_5 aerogels [23]. According to our 0D calculations, the densities of these foams are ideal, while the pore sizes are small enough to ensure good homogeneity of the lasing medium.

We performed 1D LASNEX simulations of W_2O_5 targets varying the aerogel density and laser intensity. As in the slab targets, trapping effects were included. We found densities near $\rho=0.23$ g/cm^3 irradiated with a 1-ps pulse of 2.5×10^{16} W/cm^2 to be optimal. Since the deposition region is at the gain region, i.e., near the surface, there is no need to have a short-wavelength driver. Therefore, we chose the most common driver wavelength of 1.0 μm. Although there has been very little work on aerogel absorption, we feel that assuming 10% absorption is conservative based on measured absorption of solid targets [17,18]. Shown in Fig. 4(a) is the electron density versus distance at several times. The aerogel extends from 0 to 8 μm and the laser is incident from the right. The temporal profile of the laser is Gaussian and peaked at 1.5 ps. Shown in Fig. 4(b) is the electron temperature versus distance at several times. Also shown in Fig. 4(b) is the ion temperature at 2.0 ps. As the laser is absorbed, a radiation-dominated heat front propagates into the target. The gain region moves inward following the heat front as shown in Fig. 5. However, due to the finite gain duration the

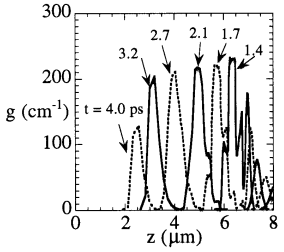

FIG. 5. Gain coefficient vs distance at several times for tungsten aerogel target.

inversion is maintained only for a short time. The result is a narrow gain region that propagates into the material. The position of the gain region is not very sensitive to laser intensity. Therefore, we anticipate that this scheme could tolerate 20% variations in intensity along the line focus.

Like the solid slab target, the gain region for the foam is narrow. However, it occurs over a much flatter density gradient. X-ray refraction in this density gradient is not as severe as in the solid slab targets. Using Eq. (2), we estimate the refraction length to be $L=300$ μm, where we have used $\nabla(n_e/n_c)\sim 10^{-5}$ $\mu\mathrm{m}^{-1}$ and $\delta z=0.5$ μm. This refraction length gives a gain length product of about $GL=6$. Gain length products less than this value have been measured for this lasing line [5]. Therefore, a flat W aerogel foam target could produce measurable signals. However, the gain length can easily be increased with a curved Lunney-type target [20]. The radius of curvature needed to overcome refraction for this foam target is 10 cm. We believe that a foam target with this large radius could easily be fabricated. Therefore, the refraction problem can be reduced and the length over which amplification can occur is determined by the line focus of the pump.

If the pump energy is sufficient to give a line focus length of 1.0 mm, then the gain length product will be $GL=20$ and the laser could reach saturation. The saturation intensity is found by equating the stimulated rate to the total exit rate R_{out} from the upper state [24]. The mean intensity at saturation is given by

$$J_s=\frac{2h\nu^3}{c^3}\frac{R_{out}}{A}, \tag{3}$$

where A is the Einstein coefficient and ν is the laser wavelength. The intensity I_s can be found by integrating over frequency. Assuming a Lorentzian profile, we find $I_s=\Delta\nu\sqrt{2\pi^3/\ln 2}J_s$, where $\Delta\nu$ is the full width at half maximum of the atomic line profile [24]. CRETIN calculates the mean intensity using the above formula and for the W_2O_5 foam we find $I_s=2.6\times 10^{12}$ (J/s)/cm^2. If we assume a transverse focus of 10 μm and we use calculated gain region width of 0.6 μm and time duration of 3 ps, we find an energy output of 0.5 μJ.

There are several experimental considerations associated with this transient scheme. First, the light travel time down the length of the laser somewhat exceeds the gain duration ($\sim$1 ps). Therefore, a traveling-wave pumping scheme is required. Such schemes already have been utilized for several extreme ultraviolet and x-ray lasers [21]. In order for the traveling wave to work, the difference in travel time down the length of the x-ray laser between x-ray laser photons (moving at the speed of light) and the front of a traveling-wave pump must be less than the gain duration. Using this criterion, we estimate that the speed of the traveling wave must be within $\pm 20\%$ of the speed of light assuming a gain duration of 0.5 ps and a line focus length of 0.5 mm. This is not a very stringent constraint and therefore would not be an experimental difficulty.

Another consideration is the uniformity of the foam target. As mentioned above, the foams have pore sizes between 20 and 50 nm. We expect that there will be sufficient density smoothing during the 1-ps pulses. Simulations show that the heat front precedes the gain region by about 1 ps. This heat front has an electron temperature of a least 1 keV. At 1-keV electron temperature the sound speed for W_2O_5 is $c_s=\sqrt{ZkT_e/M_i}\approx 2\times 10^6$ cm/s, where we have assumed $Z\sim 30$ and M_i is the mass of a W ion. Material moving at this velocity would transverse the 50-nm pore size in about 0.4 ps. Even if the main pulse is not sufficient to homogenize the foam, a modest prepulse could easily be used for density smoothing. For example, we estimate a prepulse of duration 100 ps and intensity 10^9-10^{10} W/cm^2 would be sufficient to homogenize the foam target. We note that this prepulse would not lead to much large-scale (>1 μm) hydrodynamic motion over this time duration.

IV. CONCLUSIONS

In conclusion, we predict gain coefficients exceeding 220 cm^{-1} for a 1-ps driver of intensity $I=2\times 10^{16}$ W/cm^2 using either a slab or aerogel target. Using the focal width of 10 μm and line focus of 1.0 mm, we estimate a pump energy of 2.5 J. This is attainable for many short-pulse systems; therefore, we highly recommend experiments. The conversion efficiency is $\sim 2\times 10^{-7}$, assuming 40% absorption.

ACKNOWLEDGMENTS

We thank S. Maxon for suggesting the idea of high-density ultrashort-pulse nickel-like collisional schemes and we acknowledge useful conversations with D. Eder, B. MacGowan, R. Walling, M. Rosen, R. Sheppard, L. Hrubish, and B. Hopper. Work was performed under the auspices of the U.S. Department of Energy by the Lawrence Livermore National Laboratory under Contract No. W-7405-ENG-48.

[1] R. C. Elton, *X-Ray Lasers* (Academic, New York, 1990); C. H. Skinner, Phys. Fluids B **3**, 2420 (1991).
[2] B. J. MacGowan *et al.*, Phys. Fluids B **4**, 2323 (1992), and references cited therein.
[3] M. Maxon *et al.*, J. Appl. Phys. **57**, 971 (1985): **59**, 239 (1986).
[4] S. Maxon *et al.*, Phys. Rev. A **37**, 2227 (1988); Phys. Rev. Lett. **63**, 236 (1989): **70**, 2285 (1993).
[5] B. J. MacGowan *et al.*, Phys. Rev. Lett. **65**, 420 (1990).
[6] R. A. London, M. D. Rosen, and J. E. Trebes, Appl. Opt. **28**, 3397 (1989).
[7] L. B. Da Silva *et al.*, Science **258**, 269 (1992); R. A. London *et al.*, Proc. SPIE **1741**, 333 (1993).
[8] M. D. Rosen *et al.*, Phys. Fluids **31**, 666 (1988); Phys. Rev. Lett. **54**, 106 (1985).
[9] B. E. Lemoff *et al.*, Phys. Rev. Lett. **74**, 1574 (1995).
[10] D. Eder *et al.*, Phys. Plasmas **5**, 1744 (1994).
[11] S. Moon and D. Eder, Proc. SPIE **2520**, 80 (1995).

[12] K. G. Whitney *et al.*, Phys. Rev. E **50**, 468 (1994); P. V. Nickles *et al.*, Proc. SPIE **2520**, 373 (1995).
[13] V. N. Shlyaptsev *et al.*, Proc. SPIE **2012**, 111 (1993).
[14] H. A. Scott and R. W. Mayle, Appl. Phys. B: Lasers Opt. **58**, 35 (1994).
[15] M. S. Dimitrijevic and N. Konjevic, J. Quant. Spectrosc. Radiat. Transf. **24**, 451 (1980).
[16] G. Zimmerman and W. Kruer, Comments Plasma Phys. Control. Fusion **11**, 51 (1975).
[17] D. F. Price *et al.*, Phys. Rev. Lett. **75**, 252 (1995).
[18] U. Teubner *et al.*, Phys. Plasmas **3**, 2679 (1996).
[19] M. D. Rosen, in *Proceedings of Short-Wavelength Coherent Radiation*, edited by P. H. Bucksbaum and N. M. Ceglio (Optical Society of America, Washington, DC, 1991), Vol. 11, p. 73.
[20] J. G. Lunney, Appl. Phys. Lett. **48**, 891 (1986).
[21] M. H. Sher, J. J. Macklin, J. F. Young, and S. E. Harris, Opt. Lett. **12**, 891 (1987); J. C. Moreno, J. Nilsen, and L. B. Da Silva, Opt. Commun. **110**, 585 (1994).
[22] L. W. Hrubish and R. W. Pekala, Energy Technol. Rev. **1**, 20 (1991) (available from National Technical Information Service, U.S. Dept. of Commerce, 5205 Port Royal Rd., Springfield, VA 22161 [UCRL 52000-91-1 (Jan. 1991)]); J. Livage and C. Sanchez, J. Non-Cryst. Solids **145**, 11 (1992); R. C. Mehrotra, *ibid.* **145**, 1 (1992).
[23] L. W. Hrubish (private communication).
[24] R. A. London, Phys. Fluids **31**, 184 (1988).